Epitaxial growth, dielectric response, and microstructure of compositionally graded (Ba,Sr)TiO_3 thin films grown on (100) MgO substrates by pulsed laser deposition

Xinhua Zhu,[a] Jianmin Zhu, Shunhua Zhou, Zhiguo Liu, and Naiben Ming
National Laboratory of Solid State Microstructures, Department of Physics, Nanjing University, Nanjing 210093, China

Helen Lai-Wah Chan, Chung-Loong Choy, and Kin-hung Wong
Department of Applied Physics and Materials Research Center, The Hong Kong Polytechnic University, Kowloon, Hong Kong, China

(Received 24 April 2007; accepted 19 October 2007)

Compositionally graded $(Ba_{1-x}Sr_x)TiO_3$ (BST) thin films (with $0.0 \leqslant x \leqslant 0.25$) were grown by pulsed laser deposition on the (100)MgO single-crystal substrates covered with a conductive $La_{0.5}Sr_{0.5}CoO_3$ (LSCO) layer as a bottom electrode. Their epitaxial growth, dielectric response, and microstructure were characterized. The epitaxial relationships between the BST, LSCO, and MgO can be determined as $[001]_{BST}//[001]_{LSCO}//[001]_{MgO}$ and $(100)_{BST}//(100)_{LSCO}//(100)_{MgO}$, from the x-ray diffraction (rocking curve, ϕ scans) and electron-diffraction patterns. Dielectric data showed that the room temperature values of the dielectric constant and dielectric loss of the graded BST films were 630 and 0.017 at 100 kHz, respectively. Cross-sectional transmission electron microscopy (TEM) images reveal that both the BST films and the LSCO bottom electrode grow with a columnar structure, and they have flat interfaces and overall uniform thickness across the entire specimen. Cross-sectional high-resolution TEM images reveal that at the LSCO/MgO(100) interface, an interfacial reaction is not seen, whereas edge-type interfacial dislocations with their extra half-planes residing in the LSCO side are observed with an average interval of 2.20 nm, close to the theoretical value of 2.15 nm. At/near the LSCO/BST interface, the graded BST films grow perfectly and coherently on the LSCO lattice because they have the same type of crystal structure and almost same lattice constants, and no interfacial dislocations are observed. Planar TEM images show that the graded films exhibit granular and/or polyhedral morphologies with an average grain size of 50 nm, and the aligned rectangular-shaped voids were also observed. High-resolution TEM images show that the length sizes of voids vary from 8 to 15 nm, and with width of 5 to 10 nm along the $\langle 001 \rangle$ direction in the (100) plane.

I. INTRODUCTION

$Ba_{1-x}Sr_xTiO_3$ (BST) thin films have received much attention in the microelectronic industry because of their promising applications in high-density dynamic random access memories[1–3] and microwave devices.[4–6] They exhibit not only high dielectric constant, but also good dielectric tunability,[7–10] which offers a unique opportunity to develop various microwave devices such as waveguide phase shifters,[4] decoupling capacitors,[5] and tunable filters.[6] For optimum performance of these microwave devices, the grown BST thin films should have large dielectric tunability ($[\Delta\epsilon_r/\epsilon_r]$, ϵ_r is dielectric constant), low microwave losses (or high quality factor Q), and low temperature dependence of the dielectric constants in the operational frequency range of the device and in the corresponding temperature range.[11,12]

In recent years much progress has been made in the deposition of high-quality BST films and increasing the performance of microwave devices based on BST thin films[13–17]; however, the application of BST thin films in microwave devices is still hampered by their high microwave losses and the large temperature dependence of the dielectric constants. Furthermore, there is still concern about the reliability of microwave devices over the operating frequency and temperature ranges. To match the aforementioned requirements, a simple but effective method is to prepare compositionally graded BST films

[a]Address all correspondence to this author.
e-mail: xhzhu1967@yahoo.com.cn
DOI: 10.1557/JMR.2008.0086

by depositing successive layers with different Ba/Sr ratios, where both high dielectric tunability and relatively small temperature dependence of the dielectric constant are obtained simultaneously. For example, a dielectric tunability of 65% at 444 kV/cm and temperature-insensitive dielectric property are obtained from a multilayered BST heterostructures with three different Ba/Sr ratios, which were deposited on Pt-coated Si substrates by metallorganic solution deposition.[18] For microwave tuning applications such as resonators and phase shifters that use ferroelectric films, coplanar varactor configurations are highly preferred from a design standpoint because they can be easily designed to have capacitance values that provide good impedance matching to the rest of the circuit. They are also advantageous since the epitaxial films such as BST deposited directly on single-crystal dielectric substrates (e.g., MgO, $LaAlO_3$, $NdGaO_3$), have a higher quality than the ferroelectric films deposited on metal-coated substrates.[19] However, the dielectric response and tunability of epitaxial films are closely related to the epitaxial stress within the heteroepitaxial films caused mainly by the mismatches between lattice parameters and thermal expansion coefficients of the film and substrate.[20,21]

The stress effects on the microwave dielectric properties of BST films have been experimentally investigated.[14,22–25] To optimize the microwave dielectric tunability of epitaxial BST films, Ban and Alpay[26] conducted theoretical analyses of the dielectric response as a function of the applied external electric field and the microwave dielectric tunability as a function of the misfit strain. Their results show that a high dielectric tunability can be achieved by adjusting the misfit strain especially in the vicinity of a structural phase transformation. To achieve optimum tunability, most logical approaches to manipulating the strain state in the epitaxial films are either variations of substrate materials or film thickness or variations of the deposition conditions such as oxygen ambient pressure. The misfit strain relaxation in $(Ba_{0.60}Sr_{0.40})TiO_3$ epitaxial thin films deposited on ⟨110⟩ orthorhombic $NdGaO_3$ substrates was investigated by x-ray diffraction (XRD), and the results show that two independent dislocations mechanisms operate to relieve the anisotropic misfit strains along the principal directions. The critical thicknesses for misfit dislocation formation along the [001] and [010] directions were found to be 11 and 15 nm, respectively.[27]

Recently, epitaxial BST films with compositionally graded structure grown by pulsed laser deposition have been reported, and their dielectric properties and microwave performance of tunable devices based on such graded BST thin films have been characterized.[28–34] The results show that the microwave dielectric properties of the graded BST films depended strongly on the crystalline structure and the direction of the composition gradient built in the graded BST films. However, the microstructure and interfacial structures of the graded BST films have not yet been examined in detail. This work characterizes the epitaxial growth, dielectric response, and microstructure of compositionally graded BST films grown by pulsed laser deposition (PLD) on (100)MgO single crystal substrates covered with a conductive $La_{0.5}Sr_{0.5}CoO_3$ (LSCO) bottom electrode. The epitaxial growth relationships between the BST, LSCO, and MgO single-crystal substrates are examined by XRD and selected-area electron diffraction (SAED). The dielectric properties of the graded BST films were measured by vertical structures using LSCO as the bottom electrode. Microstructure of the epitaxial graded BST films were investigated by (high-resolution) transmission electron microscopy (TEM) from both plan-view and cross-sectional specimens.

II. EXPERIMENTAL PROCEDURE

Compositionally graded $(Ba_{1-x}Sr_x)TiO_3$ films (with $0.0 \leqslant x \leqslant 0.25$) were epitaxially grown by PLD on MgO(100) single-crystal substrates covered with a conductive $La_{0.5}Sr_{0.5}CoO_3$ bottom electrode. Details of the deposition procedure are reported elsewhere.[28] However, a brief description is given here. The graded BST films were grown at 650 °C in an oxygen ambient pressure of 200 mTorr by PLD. Before deposition of the graded BST films, a LSCO bottom electrode was first deposited by PLD onto the (100)MgO substrate at 600 °C with an oxygen pressure of 150 mTorr. The graded films were in situ deposited epitaxially on the top surface of the LSCO layer. The first deposited layer for the graded BST film had the composition of $Ba_{0.75}Sr_{0.25}TiO_3$, and the last layer had $BaTiO_3$. The compositional gradients were determined by Rutherford backscattering spectroscopy (RBS; not shown here, see Ref. 28). The epitaxial growth of the compositionally graded BST films was characterized by XRD patterns, rocking curves, and ϕ scans (XRD; Philips X'Pert MRD four-circle diffractometer, Cu K_α radiation at 30 kV) (Almelo, The Netherlands) and electron-diffraction patterns. Dielectric response of the graded BST films was measured in the frequency range of 10^2 to10^6 Hz by a Hewlett-Packard (Melrose, MA) 4194A impedence analyzer with an alternating current (ac) oscillation level of 100 mV.

The microstructures of the graded BST films were examined by high-resolution TEM (HRTEM). Both cross-sectional and plan-view specimens were examined in this work. Plan-view samples were prepared by cutting disks with a diameter of 3 mm from the graded film using an ultrasonic cutter. Then these disks were ground, dimpled, and finally thinned to perforation by Gatan dual ion-milling (model 600) from the substrate side (Gatan Inc., Pleasanton, CA). Cross-sectional specimens were

prepared by cutting the sample into slices along the $(001)_{MgO}$ plane. Two slices were glued together face-to-face joining the film-covered surface. After the glue cured, disks with a diameter of 3 mm were obtained by cutting away the redundant epoxy. These disks were then ground, dimpled, and polished, followed by Ar-ion milling in a Gatan precision ion polishing system (PIPS; model 691) at 4 keV with an incident angle of 6° (Gatan Inc., Pleasanton, CA). Electron-diffraction patterns and TEM images were recorded in a Philips (Almelo, The Netherlands) CM20T electron microscope operated at 200 kV, and HRTEM investigations were performed in a JEOL (Tokyo, Japan) JEM-4000EX high-resolution electron microscope operated at 400 kV. The fast Fourier transform (FFT) pattern and the corresponding Fourier-filtered HRTEM images are obtained by using Gatan software Digital Micrography.

III. RESULT AND DISCUSSSION

A. Epitaxial growth and microstructure

Throughout this article, the crystallographic indexing is based on the following nominal unit-cell parameters: $a_{MgO} = 0.421$ nm (JCPDS No. 4-0829)[35]; LSCO has the pseudocubic perovskite-type structure with a lattice of 0.7668 nm,[36] $a_{BaTiO_3} = 0.3992$ nm; $c_{BatiO_3} = 0.4036$ nm; $a_{BST} = 0.3977$ nm (BST, $x = 0.23$); $c_{BST} = 0.3988$ nm (BST, $x = 0.23$) (for the latter two values, see the JCPDS card No. 44-0093).[35] To investigate the epitaxial growth behavior of the compositionally graded BST films, x-ray diffraction, rocking curve, and ϕ scans measurements were carried out.

Figures 1(a) and 1(b) show the θ–2θ diffraction patterns for the graded films along the normal of MgO(100) (specular) and MgO(110) (off-specular) diffraction planes, respectively. It is clearly observed in Fig. 1(a) that the prominent (100) and (200) BST reflections together with (200) peak of MgO substrate were recorded, and weak peaks of (100) and (200) LSCO reflections are also visible. This indicates that the graded BST film is highly (100)-oriented with its surface plane parallel to that of the MgO(100) substrate. Similarly, the (110) plane of the graded BST film is also parallel to that of the MgO substrate, as shown in Fig. 1(b). Figure 1(c) shows the (200) ω-scan rocking curves of BST, LSCO, and MgO, respectively. The full width at half maximum

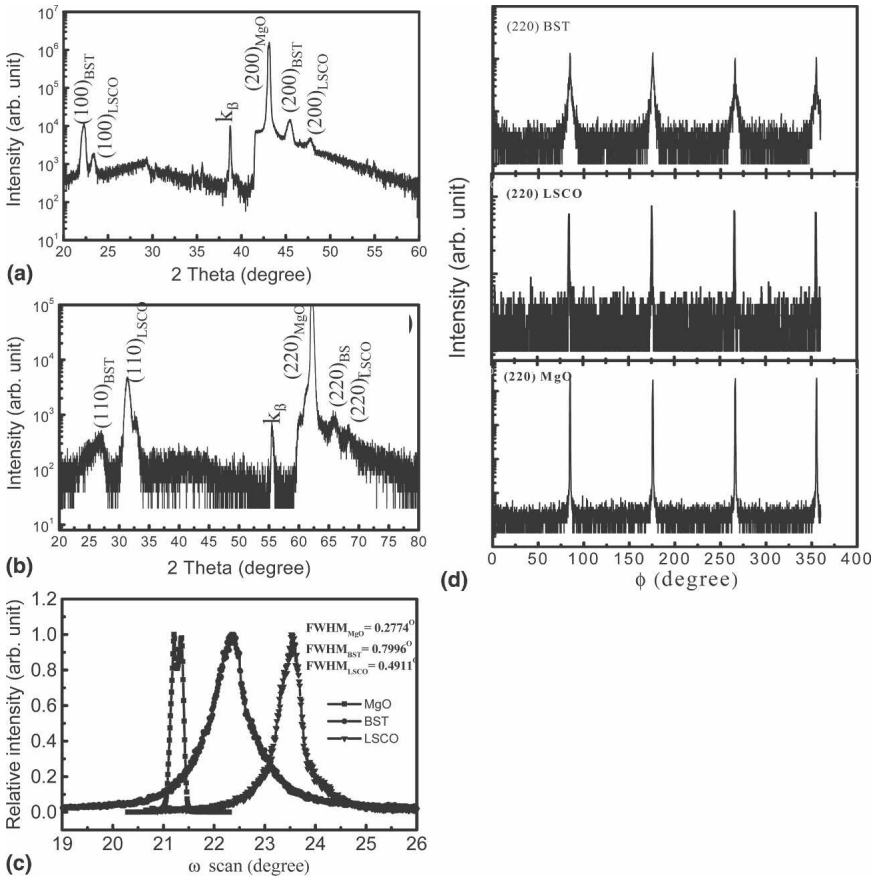

FIG. 1. Specular and off-specular XRD scans of graded BST films deposited on (100)MgO substrate with LSCO as a bottom electrode: (a) specular θ–2θ scan, (b) off-specular θ–2θ scan along the [110] direction of MgO, (c) shows the (200) rocking curves of BST, LSCO, and MgO, respectively, and (d) shows ϕ scans on the (220) reflections of BST, LSCO, and MgO, respectively.

(FWHM) of the BST (200) rocking curve, which reflects the in-plane crystalline mosaic in the film, was only about 0.8°. That indicates a small degree of mosaicity present in the graded BST film, which is also confirmed by SAED (see below). As shown in Fig. 1(b), the presence of BST (110) and (220) reflections oriented with respect to the (220) reflection of MgO displays the single-crystal nature of the grown film and reveals the in-plane epitaxial relationship between the graded BST film and the MgO substrate: $(100)_{BST}//(100)_{MgO}$ and $[001]_{BST}//[001]_{MgO}$. XRD 360° ϕ scan on the (220) reflections of BST, LSCO, and MgO, are shown in Fig. 1(d), respectively. These reflections clearly demonstrate a good epitaxial growth of the graded BST film and the LSCO bottom electrode on the (100)MgO substrate. Both the graded BST film and the LSCO bottom electrode exhibit a fourfold symmetry, indicating a cube-on-cube epitaxial growth.

To better understand the epitaxial growth behavior of the graded film, TEM investigations were also performed on the cross-sectional TEM specimen. A bright-field TEM image of the graded film, viewed from the $[001]_{MgO}$ direction is shown in Fig. 2(a), and Fig. 2(b) is the related SAED pattern taken from the graded BST film and the interface between the LSCO bottom electrode and the substrate MgO, respectively. It is observed in Fig. 2(a) that the graded film and the LSCO bottom electrode layer grow with a columnar-like structure along the $[100]_{MgO}$ direction, and the interfaces between the BST film, the LSCO bottom electrode, and the substrate are flat and very visible. The graded BST films have an overall uniform thickness across the entire specimen, but the surface roughness of the graded film is on the order of 10 nm. Some mosaic columnar texture observed in the graded BST film [see Fig. 2(a)] was caused by the rotations of grain boundaries over the entire cross-sectional sample. This is confirmed by selected-area diffraction pattern as shown in Fig. 2(b), which contains the crystallographic information for the graded film, the LSCO bottom electrode, and the MgO substrate. As clearly seen in Fig. 2(b), this diffraction pattern is a simple superposition of the graded BST film, the LSCO bottom electrode, and the MgO substrate. From the SAED pattern the reflection spots of the film, LSCO bottom electrode, and the substrate can be identified and particularly indexed using the notation of the perovskite pseudocubic basic cells. The differences in the lattice parameters in the (001) plane for BST, LSCO, and MgO can be clearly seen from the occurrence of the triple-split of {400} reflection spots along the horizontal and vertical directions, as indicated by boxes in Fig. 2(b). The enlarged ones are shown as insets in Fig. 2(b). Based on this SAED pattern, the epitaxial growth relationship between BST, LSCO, and the substrate MgO can be described as $(100)_{BST}//(100)_{LSCO}//(100)_{MgO}$ and

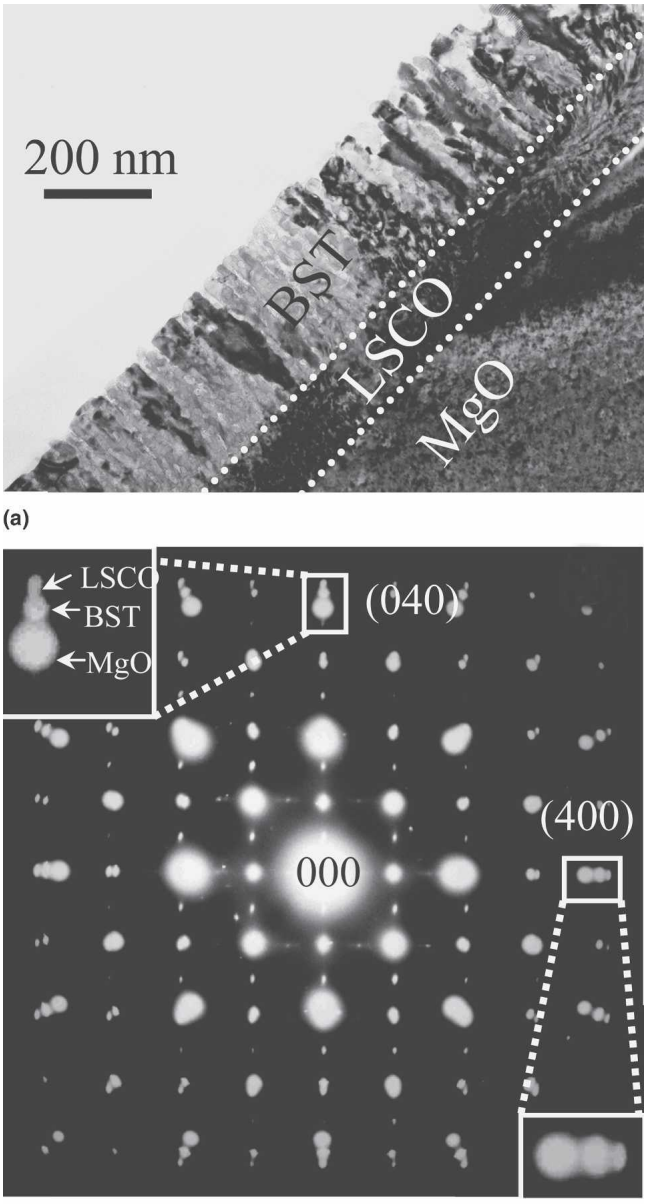

FIG. 2. (a) Bright-field cross-sectional TEM image of a graded BST film deposited on a (100)MgO single-crystal substrate, viewed along the $[001]_{MgO}$ direction. (b) Related SAED pattern taken from the graded BST film and the interface between the LSCO bottom electrode and the substrate MgO, respectively. The triple-split of the {400} reflection spots along the horizontal and vertical directions are indicated by boxes, and the enlarged ones are shown as insets in (b).

$[001]_{BST}//[001]_{LSCO}//[001]_{MgO}$, which agrees well with the above XRD.

Cross-sectional high-resolution TEM images of the interfacial regions between the MgO, LSCO, and BST film viewed from the $[001]_{MgO}$ direction, are shown in Fig. 3. Since the lattice constant for MgO is 0.421 nm, the half-lattice constant of LSCO is 0.3834 nm; so the nominal lattice mismatch δ calculated by $(a_s - a_f)/a_f$, is 9.8%, as

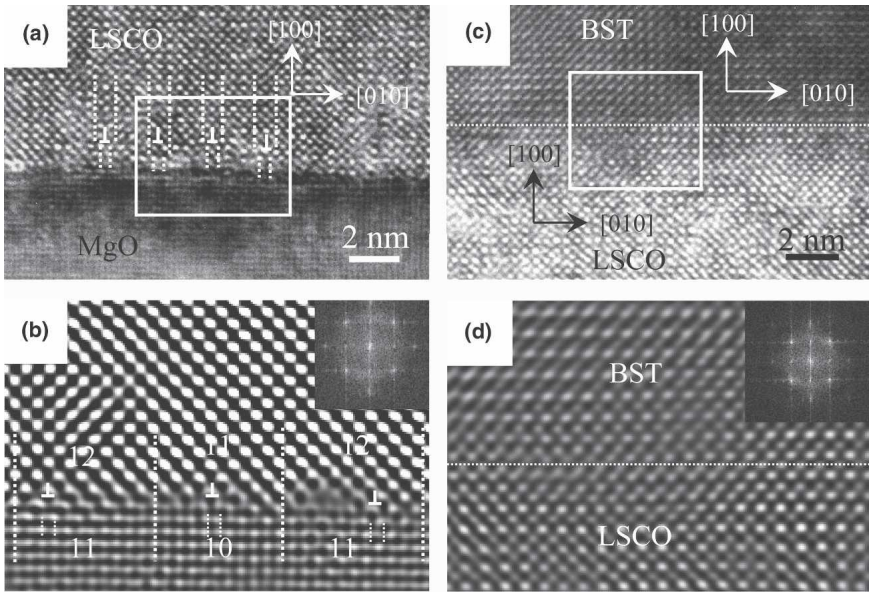

FIG. 3. Cross-sectional high-resolution TEM images of the interfacial regions between the MgO, LSCO, and BST film viewed from the $[001]_{MgO}$ direction. (a) LSCO/MgO(100) interface, some interfacial dislocations are indicated by "⊥" and (b) Fourier-filtered image of the small square area marked in (a). The numbers shown in (b) are the interplanar numbers in the MgO and the LSCO film sides. (c) BST/LSCO interface showing almost perfect coherent growth and (d) Fourier-filtered image of the small square area marked in (c). The dashed line indicates the position of the interface between the BST film and the LSCO bottom electrode. Insets in (b) and (d) are the FFT of the small square areas marked in (a) and (c), respectively.

expected at the interface, and two MgO units cells tend to be matched by a single LSCO unit. Consequently, interfacial misfit dislocations are created to release the interface strain. Misfit dislocations with an average spacing about 2.20 nm are indicated in Fig. 3(a). To clearly reveal the interfacial misfit dislocations, a Fourier-filtered image of the small square area marked in Fig. 3(a), is shown in Fig. 3(b), in which three misfit dislocations are clearly observed. The different interplanar numbers of the MgO and the LSCO film marked in Fig. 3(b) are guides to find the misfit dislocations. The misfit dislocations with their extra half-planes residing in the LSCO side occur because the interplanar distance is smaller than that of the MgO. In this case, the interplanar distances for the LSCO film and the MgO substrate are $d_1 = 0.1917$ nm (for the (400) reflection of LSCO film) and $d_2 = 0.2105$ nm (for the (200) reflection of MgO substrate). The theoretical distance (D) between two adjacent misfit dislocations is calculated to be 2.15 nm by $D = (d_1 d_2)/(d_2 - d_1)$. The measurement from Fig. 3(a) gives an average spacing about 2.20 nm for misfit dislocations, in agreement with the theoretical value. Based on the Mathews–Blakeslee criteria,[37,38] the critical thickness of LSCO film for the formation of misfit dislocation on MgO substrate is calculated to be approximately 0.43 nm. This low value of the critical thickness suggests that the misfit dislocations appear at the early nucleation and growth stage of the LSCO film.

It is naturally expected that the density of interfacial dislocations will be greatly reduced if the lattice mismatch is negligible. The nominal lattice constants for (BST, $x = 0.23$) in the (001) plane is $a = b = 0.3977$ nm, half of the lattice constant of LSCO being 0.3834 nm; therefore the nominal lattice mismatch in (001) plane for BST grown on LSCO substrate is 3.6% in the [100] and [010] directions, respectively. Actually, the lattice constants for the BST film and LSCO bottom electrode near the BST/LSCO interfacial region measured from the HRTEM image of the BST/LSCO interface [Fig. 3(c)], are 0.40 and 0.78 nm, respectively. Thus, a lattice mismatch of 2.5% appeared at the interface of BST/LSCO. Correspondingly, the interval between two adjacent dislocations is calculated to be 16 nm. A HRTEM image of the BST/LSCO interface is shown in Fig. 3(c), where the dashed line indicates the interface position. A Fourier-filtered image of the small square area marked in Fig. 3(c), is shown in Fig. 3(d), which clearly demonstrates the interfacial position. As revealed in Figs. 3(c) and 3(d), the strain field associated with the interface is rather weak so that the atom positions near the interface can be clearly resolved, and no interfacial dislocations are observed at/near the interface. It was clearly shown that the BST film grew perfectly and coherently on the LSCO (bottom electrode) lattice because they have the same type of crystal structure and almost same lattice constants.

The microstructure of the graded BST films was also examined from plan-view TEM specimen, which permits

investigation of the microstructure over a large area. Bright-field TEM image and the SAED pattern taken from a planar TEM sample are shown in Figs. 4(a) and 4(b), respectively. As shown in Fig. 4(a), the graded films exhibit granular and/or polyhedral morphologies with an average grain size of 50 nm. The SAED pattern was taken from the BST [1$\bar{2}$0] direction. The sharp diffraction spots indicate that the graded BST films have a good single-crystal quality. Furthermore, some aligned rectangular-shaped voids are also observed in the graded film. Their length varies from 8 to 15 nm with a width of 5 to 10 nm, and the orientation relationship with the surrounding BST grain is revealed by a HRTEM image, as shown in Fig. 4(b). Figure 4(c) is a Fourier-filtered image of the square area marked in Fig. 4(c) with a white line, which clearly demonstrates the orientation relationship between the void and its surrounding BST grain.

B. Dielectric response

Dielectric response of the graded BST films was measured by vertical structures using a LSCO as the bottom electrode. Variation of the dielectric constant and dielectric loss (tan δ) of the graded BST films as a function of the frequency is shown in Fig. 5. The dielectric constant and dielectric loss of the graded BST films were found to be 630 and 0.017 at 100 kHz, and 600 and ~0.022 at 1 MHz, respectively. These values are comparable to that of epitaxial $BaTiO_3$ thin films deposited on MgO substrate (dielectric constant ~500, dielectric loss of 0.05 at 100 kHz)[6] and to that of epitaxial $Ba_{0.6}Sr_{0.4}TiO_3$ thin films deposited on MgO substrate with a very thin interlayer (10 nm thickness) of $Ba_{0.9}Sr_{0.1}TiO_3$ (dielectric constant of 512, dielectric loss of ~0.02 at 1 MHz).[10] The low value of the dielectric loss in the present epitaxial graded BST film could be ascribed to the absence of high-angle grain boundaries within the graded film and no interfacial dislocations at the interface between the graded BST film and the LSCO bottom electrode. It can be seen that the dielectric constant and dielectric loss show no noticeable dispersion with the frequency, indicating the high quality of the graded film and the absence of interfacial barriers, which were confirmed by the perfect coherent growth of the BST film on LSCO bottom electrode. A tendency of a slow decrease in the dielectric constant with increasing the frequency is also observed in the present graded film, which suggests that at higher

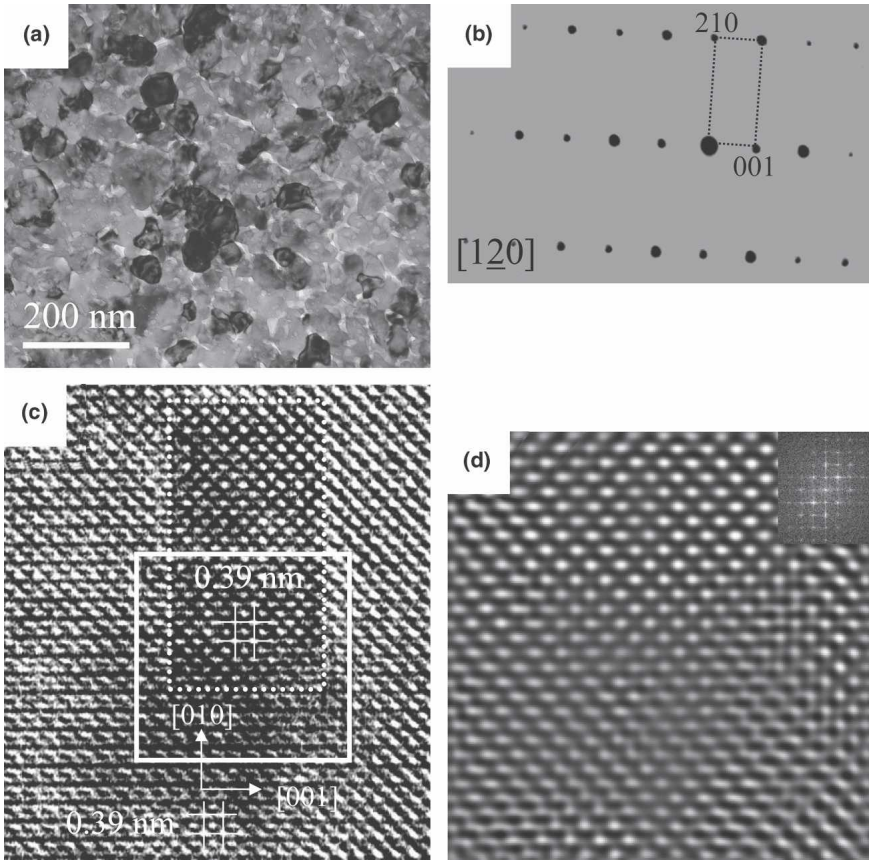

FIG. 4. (a) Bright-field TEM image and (b) the corresponding electron diffraction taken from a planar sample along the [1$\bar{2}$0] axis, and (c) a high-resolution TEM image of fine aligned rectangular-shaped voids observed in a planar BST film, and (d) an Fourier-filtered image of the area marked by a white square box in (c). Inset in (d) is the FFT pattern of the area marked by a white square in (c).

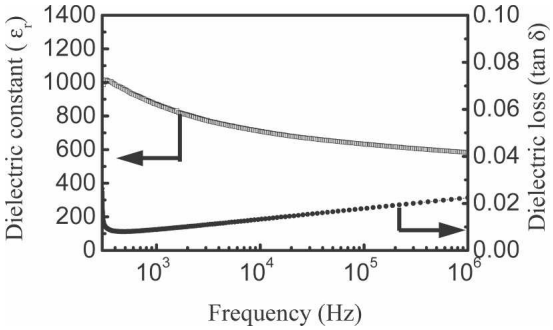

FIG. 5. Variation of dielectric constant and dielectric loss of the graded BST films as a function of the frequency.

frequency the contribution from a possible direct current conduction contribution decreases.

IV. CONCLUSIONS

Compositionally graded BST films with $0.0 \leqslant x$ 0.25 were grown by PLD on the (100)MgO single-crystal substrates covered with a conductive $La_{0.5}Sr_{0.5}CoO_3$ layer as a bottom electrode, and their epitaxial growth dielectric response, and microstructure were also examined. The epitaxial growth relationship between the BST, LSCO, and the substrate MgO can be described as $(100)_{BST}//(100)_{LSCO}//(100)_{MgO}$ and $[001]_{BST}//[001]_{LSCO}//[001]_{MgO}$ based on the XRD and SAED patterns. The dielectric constant and dielectric loss of the graded BST films were found to be 630 and 0.017 at 100 kHz. The low value of the dielectric loss observed in the present epitaxial graded BST film could be ascribed to the absence of both high-angle grain boundaries within the graded film and interfacial dislocations at the interface between the graded BST film and LSCO bottom electrode. The dielectric constant and dielectric loss show no noticeable dispersion with increasing the frequency, indicating a high quality of the graded film and the absence of interfacial barriers. Cross-sectional TEM images reveal that both the BST films and the LSCO bottom electrode grow with a columnar structure, and they have flat interfaces and overall uniform thickness across the entire specimen. High-resolution cross-sectional TEM images of the LSCO/MgO interface demonstrate the nonreactive, coherent growth of the LSCO film on the MgO substrate, and the interfacial dislocations are observed with an interval of 2.20 nm, close to the theoretical value of 2.15 nm, whereas at the BST/LSCO interface a perfect coherent growth of the BST film on the LSCO lattice was observed without any interfacial dislocation because they have the same type of crystal structure and almost the same lattice constants. Planar TEM images reveal that the graded films exhibit granular and/or polyhedral morphologies with an average grain size of 50 nm, and the aligned rectangular-shaped voids are present in the graded films. High-resolution planar TEM images show that the length sizes of voids vary from 8 to 15 nm, and with width of 5 to10 nm along the ⟨001⟩ direction in the (100) plane.

ACKNOWLEDGMENTS

This work is financially supported by Natural Science Foundation of Jiangsu Province (Project No. BK2007130), opening project Z010804 of National Laboratory of Solid State Microstructures, and National Natural Science Foundation of China under Grant Nos. 60576023 and 60636010.

REFERENCES

1. J.F. Scott: High-dielectric constant thin films for dynamic random access memories (DRAM). *Ann. Rev. Mater. Sci.* **28,** 79 (1998).
2. G.W. Dietz, M. Schumacher, R. Waser, S.K. Streiffer, C. Basceri, and A.I. Kingon: Leakage currents in $Ba_{0.7}Sr_{0.3}TiO_3$ thin films for ultrahigh-density dynamic random access memories. *J. Appl. Phys.* **82,** 2359 (1997).
3. R.E. Jones: Integration of ferroelectric nonvolatile memories. *Solid State Technol.* **40,** 201 (1997).
4. J.P. Maria, S. Trolier-McKinstry, and D.G. Schlom: *ISAF'96: Proceedings of the 10th IEEE International Symposium on Applications of Ferroelectrics*, Vol. 1 (IEEE Ultrasonics, Ferroelectrics, and Frequency Control Society, 1996), p. 333.
5. X.H. Zhu, J.M. Zhu, S.H. Zhou, Z.G. Liu, N.B. Ming, S.G. Lu, H.L.W. Chan, and C.L. Choy: Recent progress of (Ba,Sr)TiO_3 thin films for tunable microwave devices. *J. Electron. Mater.* **32,** 1125 (2003).
6. B.H. Hoerman, G.M. Ford, L.D. Kaufmann, and B.W. Wessels: Dielectric properties of epitaxial $BaTiO_3$ thin films. *Appl. Phys. Lett.* **73,** 2248 (1998).
7. W.J. Kim, H.D. Wu, W. Chang, S.B. Qadri, J.M. Pond, S.W. Kirchoefer, D.B. Chrisey, and J.S. Horwitz: Microwave dielectric properties of strained $(Ba_{0.4}Sr_{0.6})TiO_3$ thin films. *J. Appl. Phys.* **88,** 5448 (2000).
8. C.M. Carlson, T.V. Rivkin, P.A. Parilla, J.D. Perkins, D.S. Ginley, A.B. Kozyrev, V.N. Oshadchy, and A.S. Pavlov: Large dielectric constant (ϵ/ϵ_0 > 6000) $Ba_{0.4}Sr_{0.6}TiO_3$ thin films for high-performance microwave phase shifters. *Appl. Phys. Lett.* **76,** 1920 (2000).
9. W. Chang, J.S. Horwitz, A.C. Carter, J.M. Pond, S.W. Kirchoefer, C.M. Gilmore, and D.B. Chrisey: The effect of annealing on the microwave properties of $Ba_{0.5}Sr_{0.5}TiO_3$ thin films. *Appl. Phys. Lett.* **74,** 1033 (1999).
10. B.H. Park, E.J. Peterson, Q.X. Jia, J. Lee, X. Zeng, W. Si, and X.X. Xi: Effects of very thin strain layers on dielectric properties of epitaxial $Ba_{0.6}Sr_{0.4}TiO_3$ films. *Appl. Phys. Lett.* **78,** 533 (2001).
11. R.J. Cava: Dielectric materials for applications in microwave communications. *J. Mater. Chem.* **11,** 54 (2001).
12. M.W. Cole, P.C. Joshi, and M.H. Ervin: La doped $Ba_{1-x}Sr_xTiO_3$ thin films for tunable device applications. *J. Appl. Phys.* **89,** 6336 (2001).
13. C.L. Chen, J. Shen, S.Y. Chen, G.P. Luo, C.W. Chu, F.A. Miranda, F.W. Van Keuls, J.C. Jiang, E.I. Meletis, and H.Y. Chang: Epitaxial growth of dielectric $Ba_{0.6}Sr_{0.4}TiO_3$ thin film on MgO for room temperature microwave phase shifters. *Appl. Phys. Lett.* **78,** 652 (2001).
14. C.L. Canedy, H. Li, S.P. Alpay, L. Salamanca-Riba, A.L. Roytburd, and R. Ramesh: Dielectric properties in heteroepitaxial

$Ba_{0.6}Sr_{0.4}TiO_3$ thin films: Effect of internal stresses and dislocation-type defects. *Appl. Phys. Lett.* **77,** 1695 (2000).
15. M.W. Cole, W.D. Nothwang, C. Hubbard, E. Ngo, and M. Ervin: Low-dielectric loss and enhanced tunability of $Ba_{0.6}Sr_{0.4}TiO_3$ based thin films via material compositional design and optimized film processing methods. *J. Appl. Phys.* **93,** 9218 (2003).
16. D.M. Bubb, J.S. Horwitz, S.B. Qadri, S.W. Kirchoefer, C. Hubert, and J. Levy: (Ba,Sr)TiO_3 thin films grown by pulsed laser deposition with low-dielectric loss at microwave frequencies. *Appl. Phys. A* **79,** 99 (2004).
17. O. Auciello, S. Saha, D.Y. Kaufman, S.K. Streiffer, W. Fan, B. Kabius, J. Im, and P. Baumann: Science and technology of high-dielectric constant thin films and materials integration for application to high frequency devices. *J. Electroceram.* **12,** 119 (2004).
18. S. Zhang, S.P. Alpay, M.M. Cole, E. Ngo, S. Hirsch, and J.D. Demaree: High tunable and temperature insensitive multiplayer barium titanate films. *Appl. Phys. Lett.* **90,** 092901-1 (2007).
19. D. Dimos and C.H. Muller: Perovskite thin films for high-frequency capacitor applications. *Ann. Rev. Mater. Sci.* **28,** 397 (1998).
20. W. Chang, J.S. Horwitz, A.C. Carter, J.M. Pond, S.W. Kirchoefer, C.M. Gilmore, and D.B. Chrisey: The effect of annealing on the microwave properties of $Ba_{0.5}Sr_{0.5}TiO_3$ thin films. *Appl. Phys. Lett.* **74,** 1033 (1999).
21. S.B. Desu: Influence of stresses on the properties of ferroelectric $BaTiO_3$ thin films. *J. Electrochem. Soc.* **140,** 2981 (1993).
22. T.M. Shaw, Z. Suo, M. Huang, E. Liniger, R.B. Laibowitz, and J.D. Baniecki: The effect of stress on the dielectric properties of barium strontium titanate thin films. *Appl. Phys. Lett.* **75,** 2129 (1999).
23. W. Chang, C.M. Gilmore, W.J. Kim, J.M. Pond, S.W. Kirchoefer, S.B. Qadri, D.B. Chirsey, and J.S. Horwitz: Influence of strain on microwave dielectric properties of (Ba,Sr)TiO_3 thin films. *J. Appl. Phys.* **87,** 3044 (2000).
24. J.S. Horwitz, W.T. Chang, W. Kim, S.B. Qadri, J.M. Pond, S.W. Kirchoefer, and D.B. Chrisey: The effect of stress on the microwave dielectric properties of $Ba_{0.5}Sr_{0.5}TiO_3$ thin films. *J. Electroceram.* **4,** 357 (2000).
25. H. Li, A.L. Roytburd, S.P. Alpay, T.D. Tran, L. Salamanca-Riba, and R. Ramesh: Dependence of dielectric properties on internal stresses in epitaxial barium strontium titanate thin films. *Appl. Phys. Lett.* **78,** 2354 (2001).
26. Z.G. Ban and S.P. Alpay: Optimization of the tunability of barium strontium titanate films via epitaxial stresses. *J. Appl. Phys.* **93,** 504 (2003).
27. W.K. Simon, E.K. Akdogan, and A. Safari: Misfit strain relaxation in $(Ba_{0.60}Sr_{0.40})TiO_3$ epitaxial thin films on orthorhombic $NdGaO_3$ substrates. *Appl. Phys. Lett.* **89,** 022902 (2006).
28. X.H. Zhu, H.L.W. Chan, C.L. Choy, and K.H. Wong: Epitaxial growth and dielectric properties of functionally-graded $(Ba_{1-x}Sr_x)TiO_3$ thin films with stoichiometric variation. *J. Vac. Sci. Technol., A* **20,** 1796 (2002).
29. X.H. Zhu, N. Chong, H.L.W. Chan, C.L. Choy, Z.G. Liu, and N.B. Ming: Epitaxial growth and planar dielectric properties of compositionally graded $(Ba_{1-x}\ Sr_x)TiO_3$ thin films prepared by pulsed laser deposition. *Appl. Phys. Lett.* **80,** 3376 (2002).
30. X.H. Zhu, S.G. Lu, H.L.W. Chan, C.L. Choy, and K.H. Wong: Microstructures and dielectric properties of compositionally graded $(Ba_{1-x}Sr_x)TiO_3$ thin films prepared by pulsed laser deposition. *Appl. Phys. A.* **76,** 225 (2003).
31. S.G. Lu, X.H. Zhu, C.L. Mak, K.H. Wong, H.L.W. Chan, and C.L. Choy: High tunability in compositionally graded epitaxial barium strontium titanate thin films by pulsed laser deposition. *Appl. Phys. Lett.* **82,** 2877 (2003).
32. S.J. Lee, S.E. Moon, H.C. Ryu, M.H. Kwak, Y.T. Kim, and S.K. Han: Microwave properties of compositionally graded (Ba,Sr)TiO_3 thin films according to the direction of the composition gradient for tunable microwave applications. *Appl. Phys. Lett.* **82,** 2133 (2003).
33. S.J. Lee, S.E. Moon, M.H. Kwak, H.C. Ryu, Y.T. Kim, and S.K. Han: Microwave properties of compositionally graded (Ba,Sr)TiO_3 thin films for electrically tunable microwave devices. *Integr. Ferroelectr.* **49,** 151 (2002).
34. X.H. Zhu, J.M. Zhu, S.H. Zhou, Z.G. Liu, N.B. Ming, H.L.W. Chan, C.L. Choy, K.H. Wong, and D. Hesse: Microstructure and dielectric properties of compositionally-graded $(Ba_{1-x}Sr_x)TiO_3$ thin films. *Mater. Sci. Eng., B* **118,** 219 (2005).
35. JCPDS Nos. 4-0829 and 44-0093. International Center for Diffraction Data: Newton Square, PA, 2001.
36. F.S. Galasso: *Structure, Properties and Preparation of Perovskite-type Compounds* (Pergamon Press, Oxford, 1969), Chap. 1.
37. J.W. Mathews and A.E. Blakeslee: Defects in epitaxial multilayers: I. Misfit dislocations. *J. Cryst. Growth* **27,** 118 (1974).
38. R. People and J.C. Bean: Calculation of critical layer thickness versus lattice mismatch for Ge_xSi_{1-x}/Si strain-layer heterostructures. *Appl. Phys. Lett.* **47,** 322 (1985).